Electronic Supplementary Information (ESI)

Low-temperature synthesis of Mn-based mixed metal oxides with novel fluffy structures as efficient catalysts for selective reduction of nitrogen oxides by ammonia

Bo Meng,[a] Zongbin Zhao,*[a] Yongsheng Chen,[b] Xuzhen Wang[a], Yong Li[c] and Jieshan Qiu*[a]

[a] Carbon Research Laboratory, Liaoning Key Lab for Energy Materials and Chemical Engineering, PSU-DUT Joint Center for Energy Research, State Key Lab of Fine Chemicals, Dalian University of Technology, Dalian 116024, China.

[b] EMS Energy Institute, PSU-DUT Joint Center for Energy Research, and John and Willie Leone Family Department of Energy and Mineral Engineering, the Pennsylvania State University, University Park, PA, 16802, USA

[c] State Key Laboratory of Catalysis, Dalian Institute of Chemical Physics, Chinese Academy of Sciences, Dalian, China.

**Corresponding author: E-mail address: zbzhao@dlut.edu.cn, jqiu@dlut.edu.cn.*

1. Experimental details

1.1 Synthesis of Mn-based mixed metal oxide catalysts

To prepare Co-Mn-O, 0.0133 mol manganese chloride tetrahydrate and 0.0067 mol cobalt acetate tetrahydrate (or ferrous chloride tetrahydrate for Fe-Mn-O, or nickel acetate tetrahydrate for Ni-Mn-O) were dissolved into 60 ml of ethylene glycol and the mixture was gradually cooled to -10 ^{o}C under vigorous stirring (N_2 protection) and maintained at the same temperature for 30 min. An aqueous Na_2CO_3 (200 ml, 0.2 M) solution was slowly added (1.2 ml/min) and the slurry was further aged for 1 h. After filtration and being washed with deionized water, the obtained solid was dried at 60

^{o}C and calcined at 450 ^{o}C for 4 h in air. The as-prepared Mn-based mixed metal oxide catalysts containing Co^{2+}, Fe^{2+} and Ni^{2+} were denoted hereinafter as Co-Mn-O-10, Fe-Mn-O-10 and Ni-Mn-O-10, respectively.

Synthesis of manganese oxide catalysts: 0.02mol manganese chloride tetrahydrate were used as the sole manganese source only. The synthesis procedure was same as that of the Mn-based mixed metal oxide catalysts mentioned above. The as-prepared manganese oxides were denoted hereinafter as MnO_x-10.

For comparison, cobalt oxide, iron oxide and nickel oxide catalysts were also synthesized using the same method. 0.02mol cobalt acetate tetrahydrate, 0.02mol ferrous chloride tetrahydrate, 0.02mol nickel acetate tetrahydrate were used as cobalt, iron and nickel source, respectively. The as-prepared products were denoted as Co_3O_4-10, Fe_2O_3-10 and NiO-10, respectively.

In addition, Mn-based mixed metal oxide catalysts were also synthesized by co-precipitation at 60 ^{o}C and 160 ^{o}C for comparison. The as-obtained Mn-based mixed metal oxide catalysts were denoted as Co-Mn-O+60 and Co-Mn-O+160, Fe-Mn-O+60 and Fe-Mn-O+160, Ni-Mn-O+60 and Ni-Mn-O+160, respectively.

1.2 Catalyst characterization

The morphology and structure of the as-prepared products were analyzed using transmission electron microscopy (TEM) (JEM- 2000EX, 120kV), high-resolution transmission electron microscope (HRTEM) (FEI Tecnai G2 F30, 300kV) and field emission scanning electron microscopy (FE-SEM, S-4800).

The crystal structure of the catalysts was determined by X-ray powder diffraction

(XRD). XRD patterns were recorded on a D/MAX 2400 X-ray diffractometer (Rigaku), using Cu-Kα radiation operated at 40 kV and 100 mA.

The BET surface areas of the samples were calculated from a multipoint BET analysis of the nitrogen adsorption isotherms which were performed using a Micromeritics ASAP 2020 instrument operated at -196^{o}C.

The surface compositions of the catalysts were determined by x-ray photoelectron spectroscopy (XPS). XPS spectra were collected on a Thermo ESCALAB 250 spectrometer using Al Kα x-rays as the excitation source. The binding energy of C 1s (284.6 eV) was used as an internal standard.

H_2 Temperature-programmed reduction (H_2-TPR) was performed using a ChemBet TPR instrument. In a typical run, 50 mg sample was first heated to 450 ^{o}C under 5% O_2/He (10 ml/min) to remove any adsorbed species. After cooling down to 50 ^{o}C, the sample was exposed to 8% H_2/Ar (50 ml/min) and the temperature was subsequently raised from 50 ^{o}C to 650 ^{o}C with a ramp rate of 10 ^{o}C/min.

NH_3 temperature-programmed desorption (NH_3-TPD) was performed using a ChemBet TPD instrument. In a typical run, 50 mg sample was first heated to 450 ^{o}C under 5 % O_2/He (10 ml/min) to remove any adsorbed species. After cooling down to 25^{o}C, the sample was exposed to a gas mixture of 10 %NH_3/He with a flow rate of 100 ml/min for 1 h. After purging with He at a flow rate of 100 ml/min for 1 h, the NH_3-TPD is recorded from 25 ^{o}C to 400 ^{o}C with a temperature ramp of 5 ^{o}C/min.

1.3 Catalytic activity evaluation

The NH_3-SCR reaction was performed in a continuous-flow fixed-bed quartz

reactor (8 mm i.d.) under atmospheric pressure. 200 mg (40-60 mesh) sample was loaded into the reactor, and the reactant gases (400 ppm NO, 400 ppm NH_3, 2% O_2, balanced with nitrogen) were passed through the reactor at a flow rate of 100 ml/min, GHSV = 30,000 $ml.g^{-1}.h^{-1}$. The concentrations of NO, NO_2 and O_2 in the inlet and outlet streams were monitored by an online flue gas analyzer (KM9106 Quintox, Kane International Limited) equipped with NO, NO_2 and O_2 sensors.

The N_2 and N_2O selectivities as a function of temperature and time on stream in the NH_3-SCR reaction was systematically investigated by means of using mass spectrometer (OmniStar GSD320) to continuously online detect the possible nitrogen-containing species in the outlet stream. Typically, the feed gas contained 500 ppm NO, 500 ppm NH_3, 2% O_2, balanced with He, GHSV = 30,000 $ml.g^{-1}.h^{-1}$.

2. Supplementary XRD patterns, Fe-SEM, HRTEM and TEM images, XPS spectra and catalytic experimental results

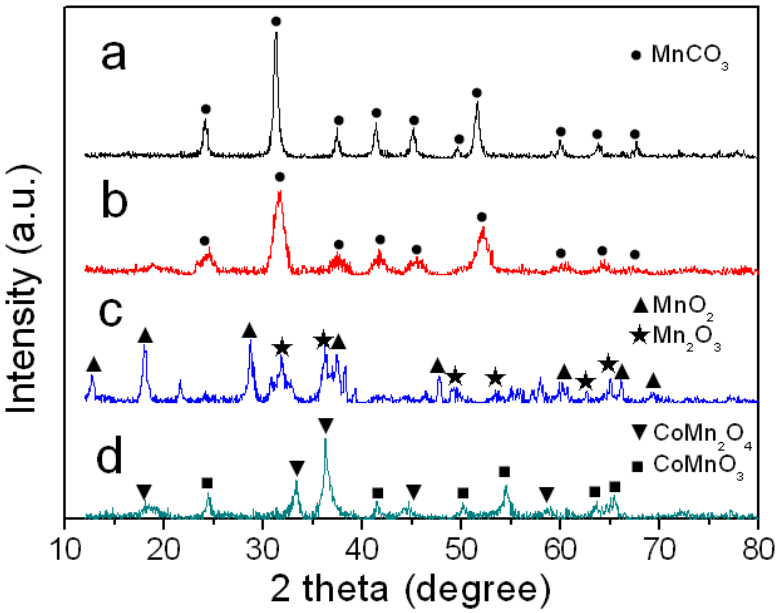

Fig. S1. XRD patterns of the precipitates of (a) manganese, (b) manganese-cobalt at -10 °C and the corresponding calcined samples (c) MnO_x-10, (d) Co-Mn-O-10

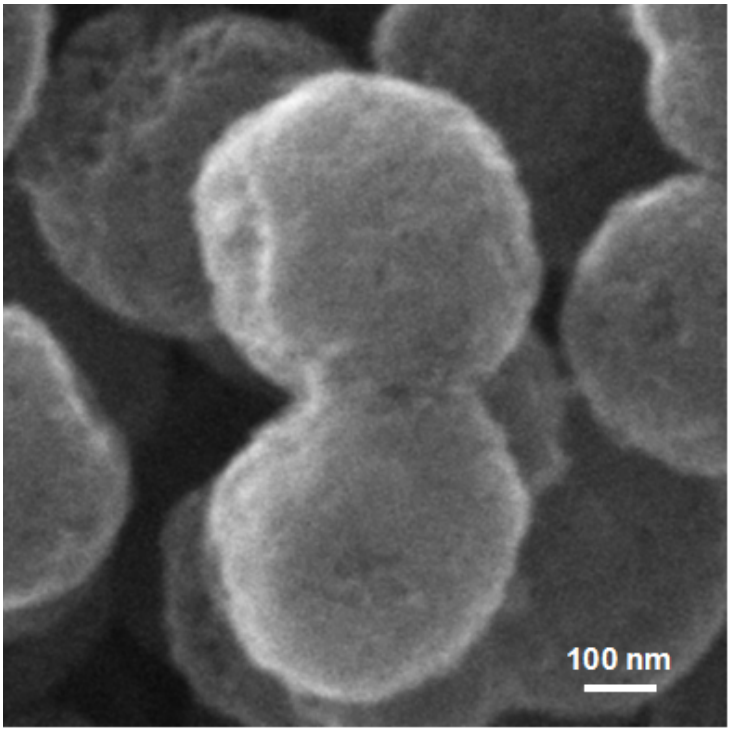

Fig. S2. FE-SEM image of MnO_x-10 catalyst.

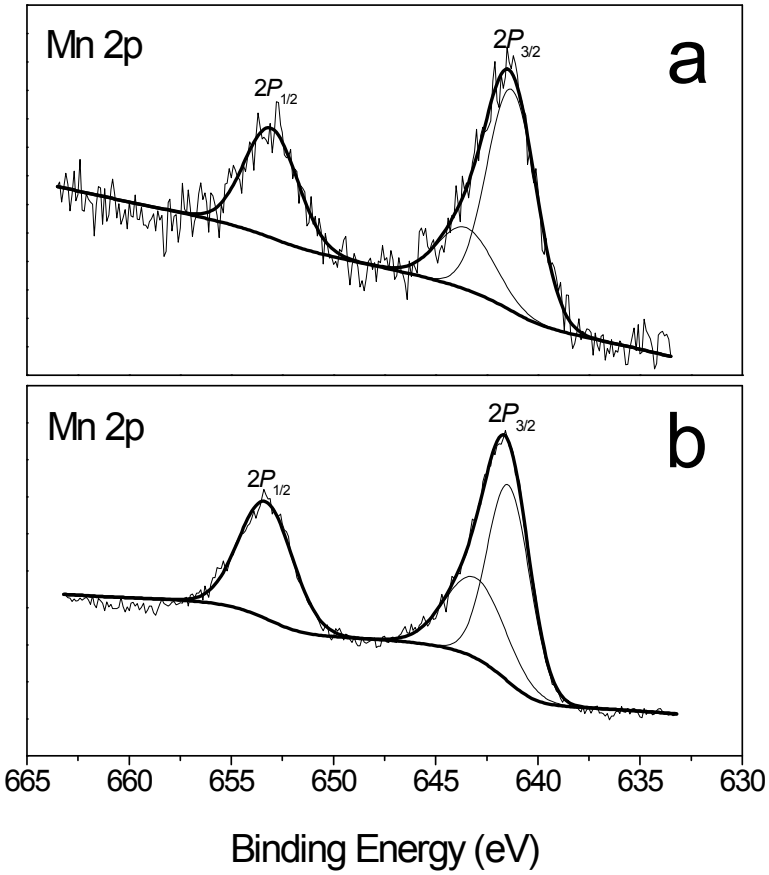

Fig. S3. Mn 2p spectra recorded from (a) MnO_x-10 and (b) Co-Mn-O-10 catalysts.

Table S1 Mn2p binding energies of MnO_x-10 and Co-Mn-O-10 catalysts

Catalysts	Mn $2p_{3/2}$ (eV)		Mn $2p_{1/2}$ (eV)
	Mn^{4+}	Mn^{3+}	
MnO_x-10	643.7	641.3	653.2
Co-Mn-O-10	643.3	641.5	653.3

For MnO_x-10 and Co-Mn-O-10 catalysts, the Mn $2p_{3/2}$ spectra show a main peak at 641 eV and a secondary peak at 643 eV (Fig. S3 and Table S1). The principal peak at 641 eV results from the contribution of Mn^{3+} ions, while the peak at 643 eV demonstrates the presence of Mn^{4+} ions[1]. This confirms that MnOx-10 catalysts are a mixture of Mn_2O_3 and MnO_2 oxides and the major constituent of the Co-Mn-O-10 catalysts are $CoMn_2O_4$ and $CoMnO_3$.

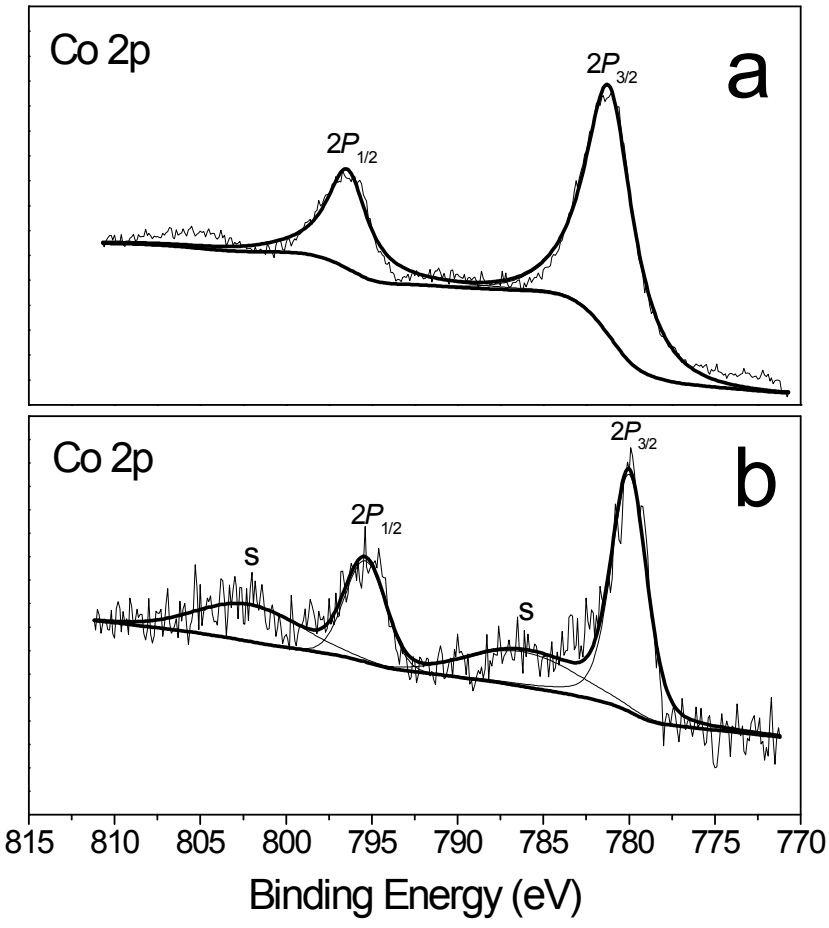

Fig. S4. Co 2p spectra recorded from (a) Co_3O_4-10 and (b) Co-Mn-O-10 catalysts.

Table S2. Co2p binding energies of Co_3O_4-10 and Co-Mn-O-10 catalysts.

Catalysts	Co $2p_{3/2}$ (eV)	Satellite (eV)	Co $2p_{1/2}$ (eV)	Satellite (eV)
Co_3O_4-10	781.2	-	796.5	-
Co-Mn-O-10	780.0	786.2	795.4	802.2

As shown in Fig. S4 and Table S2, the Co_3O_4-10 catalysts have binding energies around 781.2 eV and 796.5 eV for Co $2p_{3/2}$ and Co $2p_{1/2}$, respectively. The surface of Co_3O_4 spinel structure is comprised of low spin, diamagnetic Co^{3+} in octahedrally coordinated sites and Co^{2+} in tetrahedrally coordinated sites. The Co 2p spectra of Co-Mn-O-10 catalysts show peaks around 780.0 eV with the satellite around 786.2, and 795.4 eV with the satellite around 802.2 eV, due to Co $2p_{3/2}$ and Co $2p_{1/2}$, respectively. The peaks and their intense shake-up satellites are typical for high spin Co^{2+} ions[2-4], which is consistent with the their XRD patterns (Fig.S1) that their major constituents are $CoMn_2O_4$ and $CoMnO_3$.

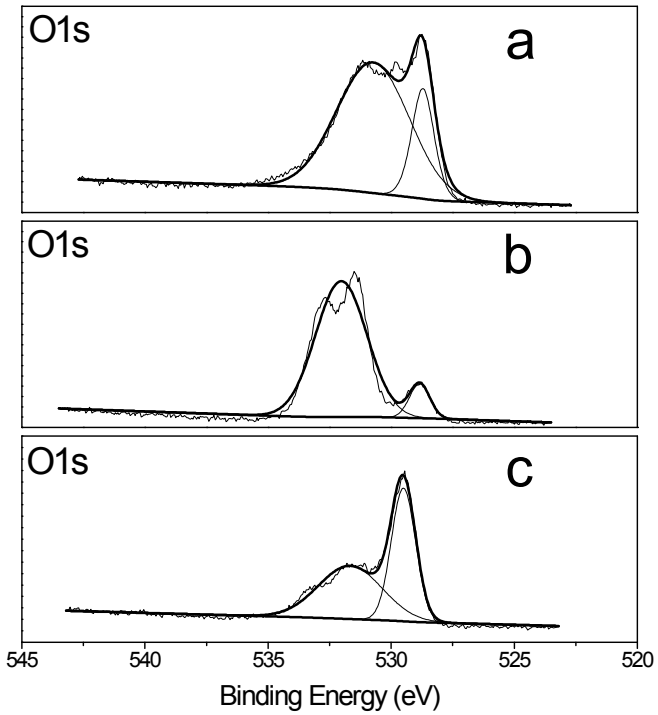

Fig. S5. O1s spectra recorded from (a) Co_3O_4-10, (b) MnO_x-10 and (c) Co-Mn-O-10 catalysts.

Table S3 O1s binding energies of Co_3O_4-10, MnO_x-10 and Co-Mn-O-10 catalysts.

Catalysts	O1s (eV)		lattice oxygen/ surface-adsorbed oxygen
	lattice oxygen	surface-adsorbed oxygen	
Co_3O_4-10	528.7	530.8	0.29
MnO_x-10	528.8	532.0	0.10
Co-Mn-O-10	529.5	531.7	0.82

The O1s spectra recorded from Co_3O_4-10, MnO_x-10 and Co-Mn-O-10 catalysts were deconvoluted into two peaks (Fig. S5 and Table S3). The first peak appearing at 529 eV can be assigned to the lattice oxygen and therefore correspond to Co-O and Mn-O[5]. The second peak at around 531 eV can be attributed to the surface-adsorbed oxygen such as O_2^{2-} or O^-, in the form of hydroxyl, OH^-, and carbonate, CO_3[1-2, 5]. The value of the lattice oxygen/surface-adsorbed oxygen ratio was calculated by dividing the area of the lattice oxygen peak by the area of the surface-adsorbed oxygen peak. According to the calculation result, compared with Co_3O_4-10 and MnO_x-10 catalysts, there are more lattice oxygen distributed on the surface of Co-Mn-O-10 catalysts.

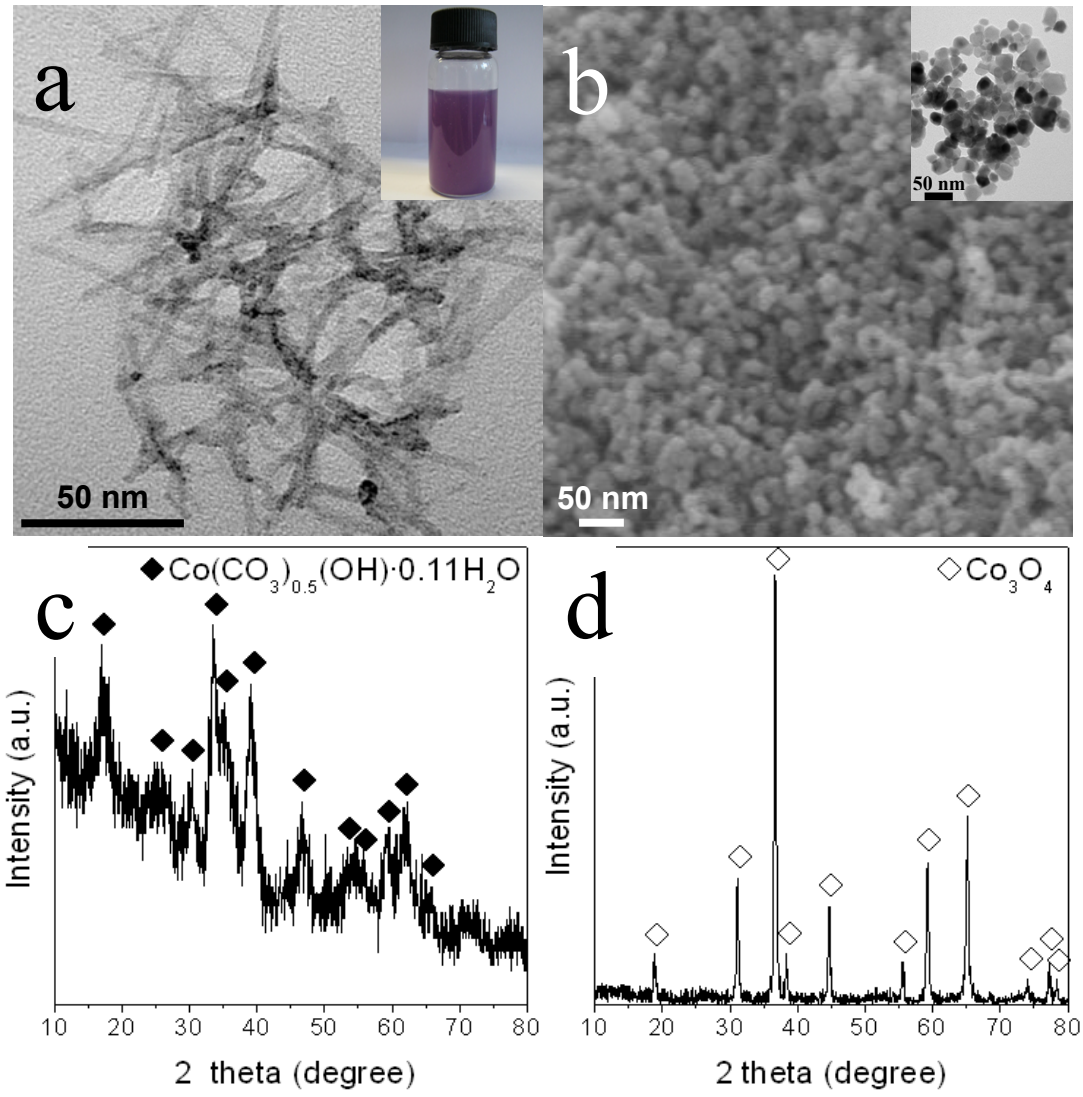

Fig. S6. (a) TEM and digital (inset) images of Co precipitate at -10°C; (b) FE-SEM and TEM (inset) images of Co_3O_4-10 catalysts; (c) XRD pattern of the Co precipitate at -10°C; (d) XRD pattern of Co_3O_4-10 catalysts.

When the Co^{2+} cations dissolved in ethylene glycol and reacted with aqueous sodium carbonate solution at -10°C, a purple precipitate was formed (Fig. S6a, inset). The TEM image of the as-obtained precipitates (Fig. S6a) reveals that their morphology is nanorods, with straight sides and regular ends, about 4nm in diameter and 50nm in length. Their XRD pattern (Fig. S6c) shows that they can be indexed to cobalt carbonate hydroxide hydrate $Co(CO_3)_{0.5}(OH)\cdot 0.11H_2O$ (JCPDS No. 48-0083).

After calcining at 450°C for 4h in air, the Co_3O_4-10 catalysts were obtained. The FE-SEM (Fig. S6b) and TEM (Fig. S6b, inset) images of the Co_3O_4-10 catalysts demonstrate that nanorods precursor had completely transformed into nanoparticles with the diameters in the range of 10-20nm after calcination. The XRD pattern of the Co_3O_4-10 catalysts (Fig. S6d) shows that they can be indexed to tricobalt tetraoxide Co_3O_4 (JCPDS No. 78-1970). The BET surface area of these Co_3O_4 nanoparticles is 52.6m^2/g.

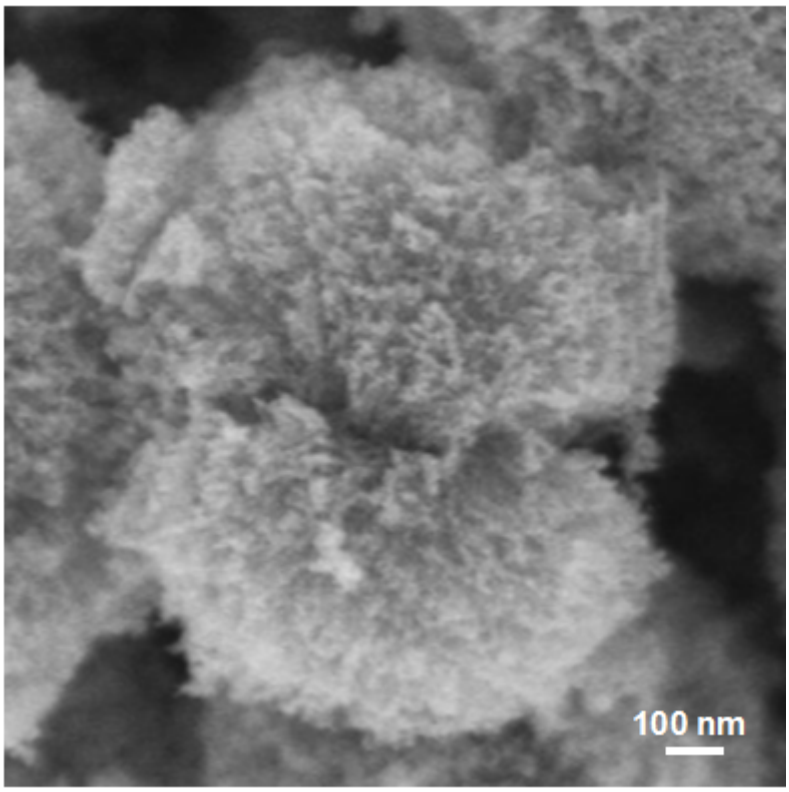

Fig. S7. FE-SEM image of Co-Mn-O-10 catalyst.

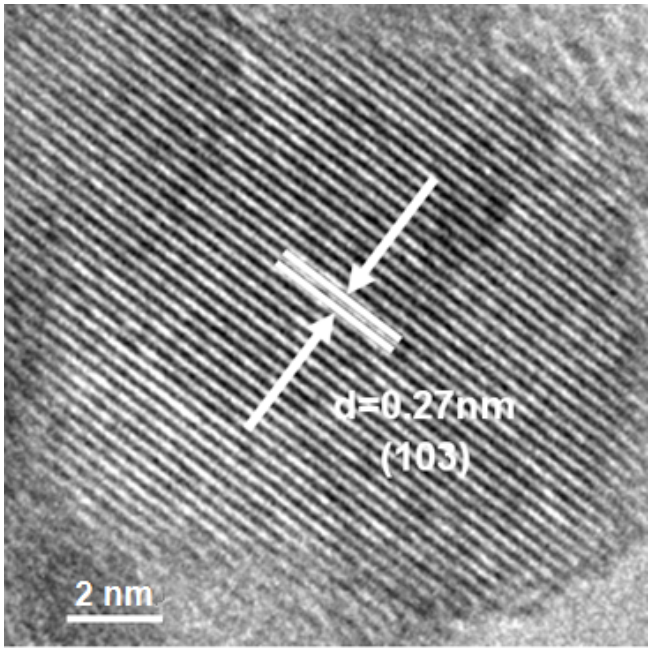

Fig. S8. HRTEM image of Co-Mn-O-10 catalyst.

From the HRTEM image of the Co-Mn-O-10 catalyst, the (103) lattice spacing (0.27 nm) of tetragonal $CoMn_2O_4$ can be clearly observed[6].

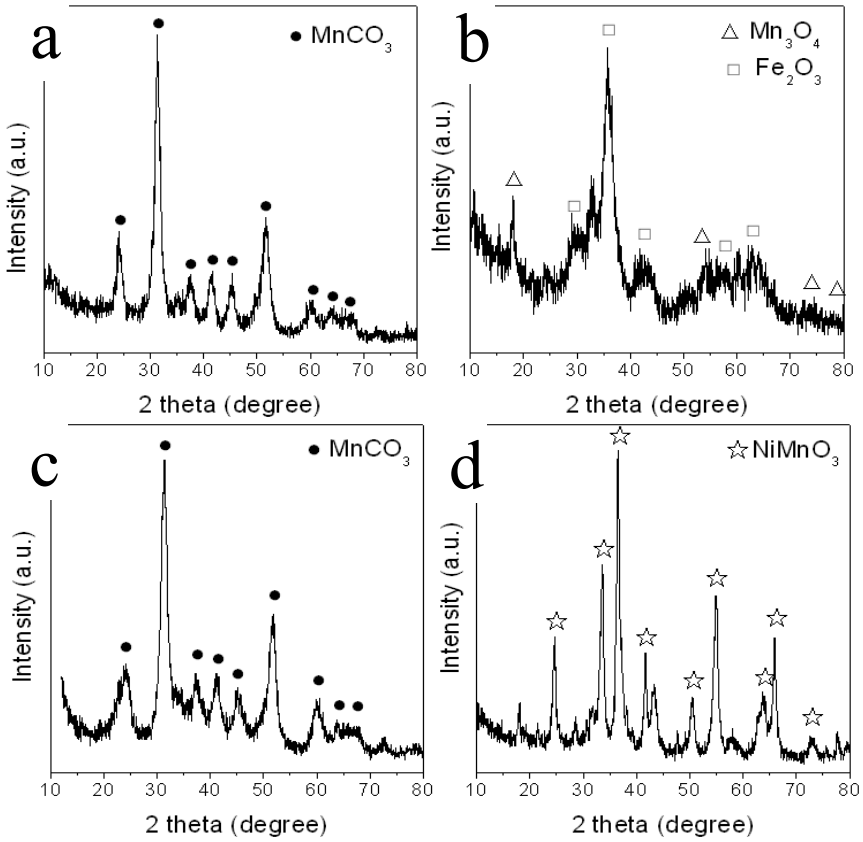

Fig. S9. XRD pattern of (a) Fe/Mn precipitate at -10 °C, (b) Fe-Mn-O-10 catalysts, (c) Ni/Mn

precipitate at -10 °C and (d) Ni-Mn-O-10 catalyst

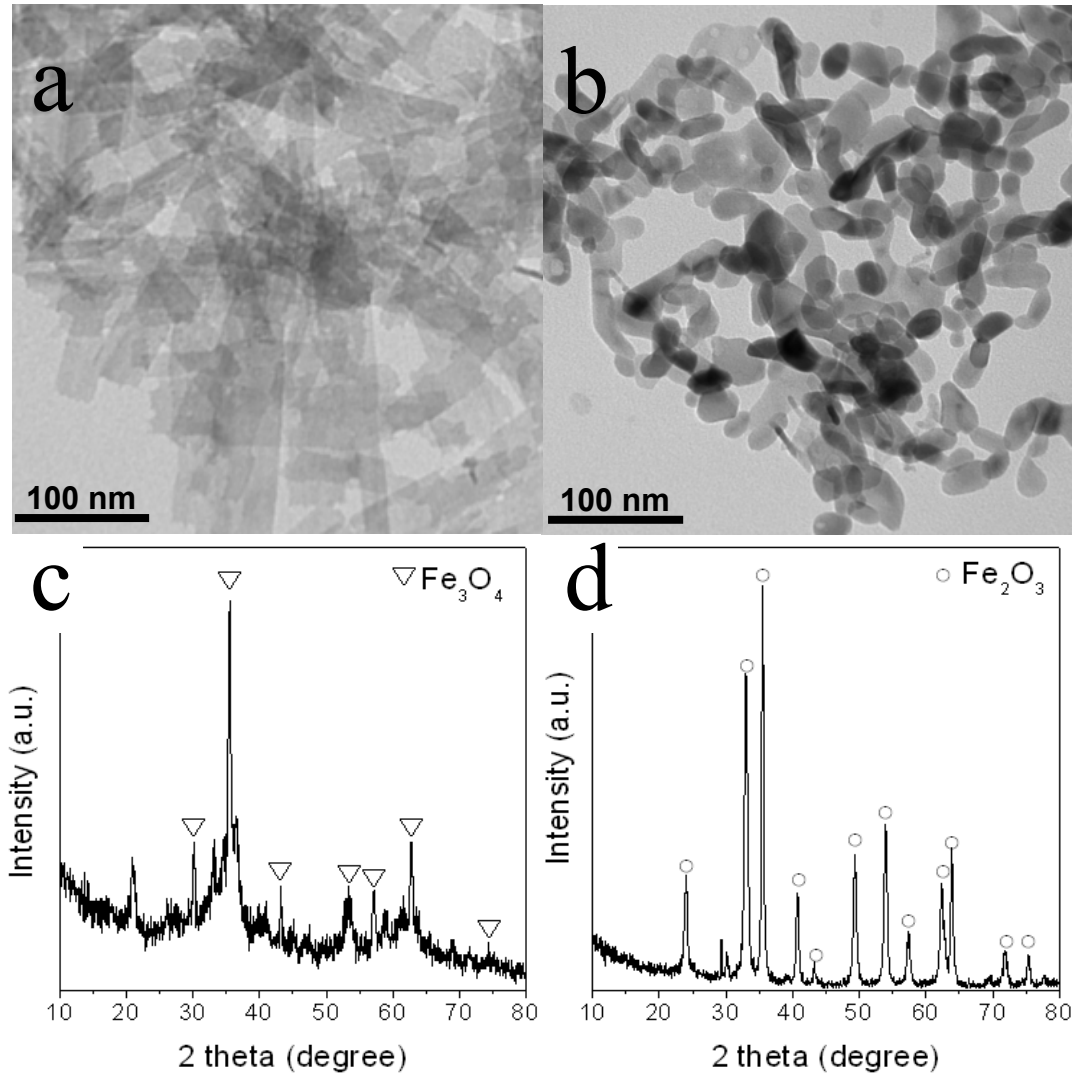

Fig S10. (a) TEM image of Fe precipitate at -10°C; (b) TEM image of Fe_2O_3-10; (c) XRD pattern of the Fe precipitate at -10°C; (d) XRD pattern of Fe_2O_3-10.

The TEM image of the Fe precipitate obtained at -10°C (Fig. S10a) reveals that their morphology is nanobelts, about 30nm in diameter and 180nm in length. When the Fe precipitate was washed and dried at 60°C, their XRD pattern (Fig. S10c) shows that they can be indexed to Fe_3O_4 (JCPDS No. 75-0033). One possible reason for this result is that the initial precipitated product ferrous hydroxide is decomposed and oxidized to ferroferric oxide in the drying process. After calcining at 450°C for 4h in air, the Fe_2O_3-10 catalysts were obtained. The TEM (Fig. S10b) image of the Fe_2O_3-

10 catalysts demonstrates that the nanobelts have transformed into nanoparticles with the diameters in the range of 20-40nm after calcination. The XRD pattern of the Fe_2O_3-10 catalysts (Fig. S10d) shows that they can be indexed to Fe_2O_3 (JCPDS No. 72-0469). The BET surface area of these Fe_2O_3 nanoparticles is 41.2m^2/g.

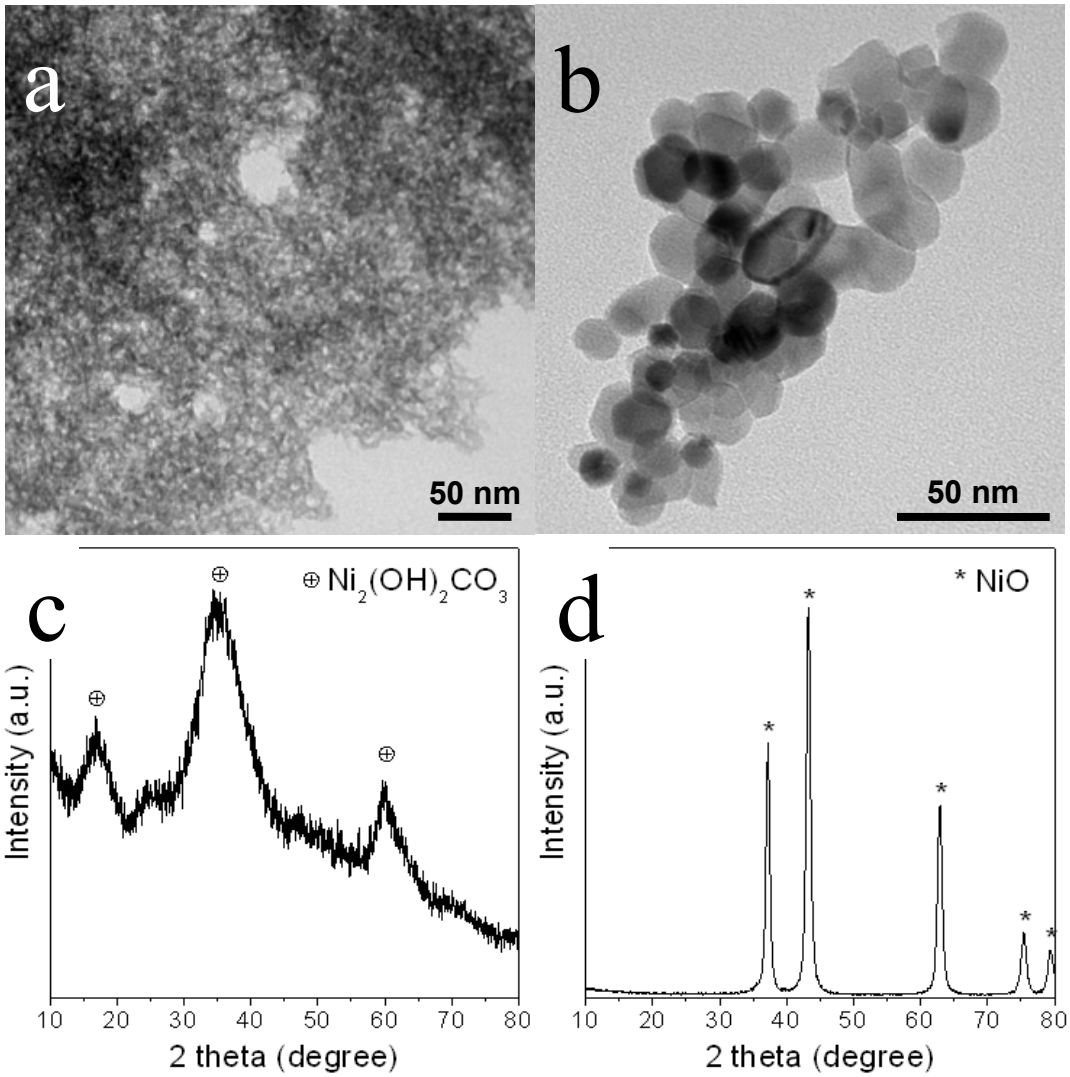

Fig. S11. (a) TEM image of Ni precipitate at -10°C; (b) TEM image of NiO-10; (c) XRD pattern of the Ni precipitate at -10°C; (d) XRD pattern of NiO-10.

The TEM image of the Ni precipitates (Fig. S11a) reveals that they have a flocculent structure. Their XRD pattern (Fig. S11c) shows that they can be indexed to $Ni_2(OH)_2CO_3 \cdot 4H_2O$ (JCPDS No. 38-0714). After calcining at 450°C for 4h in air, the NiO-10 catalysts were obtained. TEM image (Fig. S11b) demonstrates that their

morphology is nanoparticles with the diameters in the range of 10-20nm. The XRD pattern of the NiO-10 catalysts (Fig. S11d) shows that they can be indexed to NiO (JCPDS No. 47-1049). The BET surface area of these NiO nanoparticles is 65.8m^2/g.

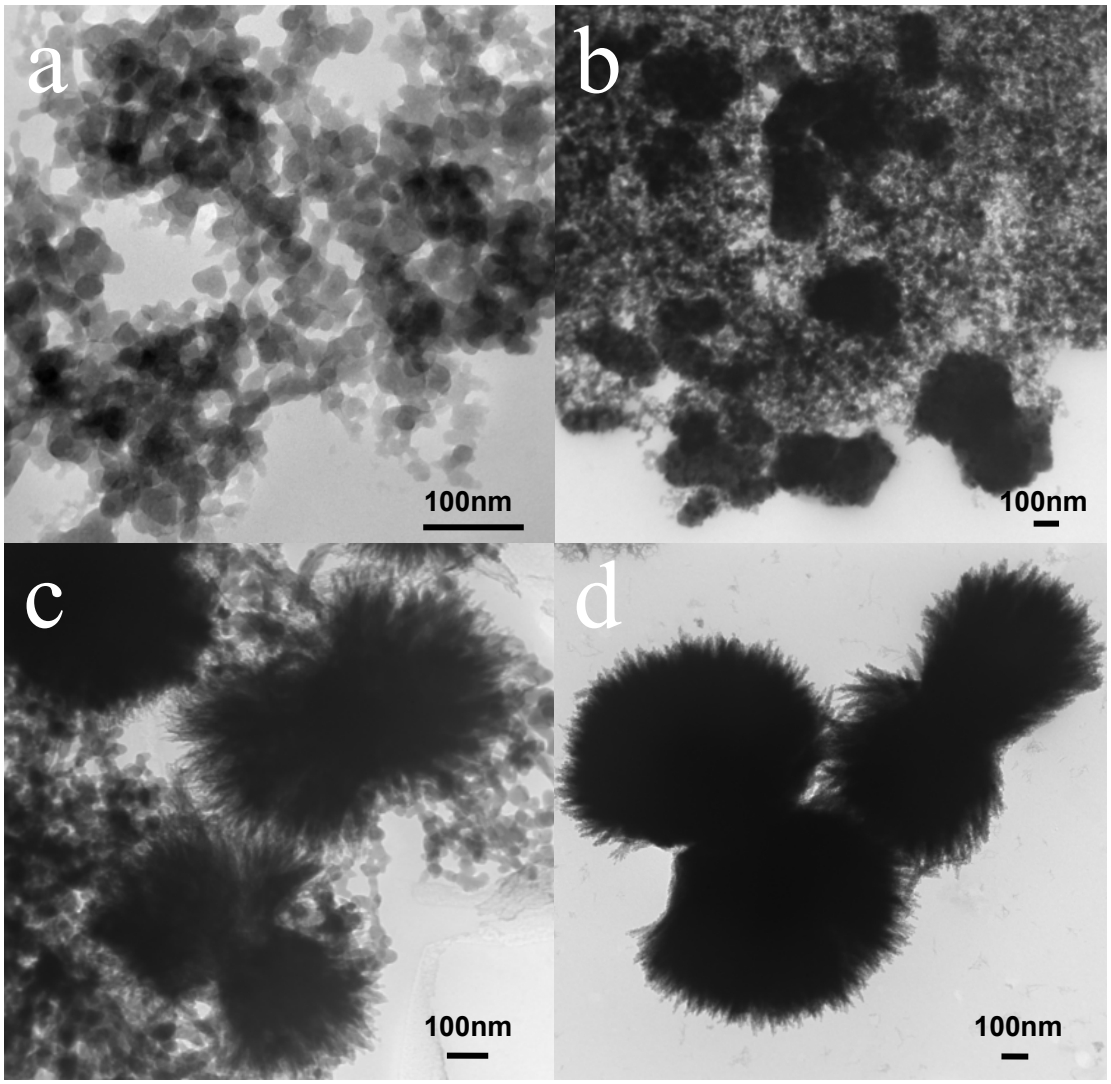

Fig. S12.TEM images of the precipitates of manganese-cobalt precursors obtained at -10 ^oC with the addition of aqueous Na_2CO_3 solutions for (a) 40 min, (b) 80 min, (c) 160 min and (d) the precursor aged for 1 h after precipitation.

The morphological evolution of Co-Mn precipitate during growth was investigated and the results are shown in Fig. S12. When the co-precipitation of Co^{2+} and Mn^{2+} ions took place for 40 min, small particles with a diameter around 20 nm were found

in the co-precipitation system (Fig. S12a). After 80 min of co-precipitation (Fig. S12b), more precipitate particles were formed and agglomeration appeared. When the co-precipitation process proceeded to 160 min, slender whiskers were observed growing on the agglomerate surface (Fig. S12c). The striking multi-whisker precipitates were obtained after the co-precipitation and further aging for 1h (Fig. S12d).

Table S4 NH_3-SCR reaction rates normalized by catalyst surface areas

Catalysts	S_{BET} ($m^2.g^{-1}$)	$Rs\times10^{10}$ ($mol.s^{-1}.m^{-2}$)		
		50°C	75°C	100°C
Co-Mn-O-10	153.5	4.9	8.1	8.5
Co_3O_4-10	52.6	0.3	0.8	0.7
Fe-Mn-O-10	148.8	4.1	7.2	8.4
Fe_2O_3-10	41.2	1.4	1.1	1.0
Ni-Mn-O-10	85.1	4.2	7.3	12.9
NiO-10	65.8	0.2	0.3	0.3
MnO_x-10	32.9	2.2	4.9	7.6

The SCR reaction rates normalized by surface areas over Mn-based mixed metal oxide and Co_3O_4-10, Fe_2O_3-10, NiO-10, MnO_x-10 catalysts have been calculated as follows[7]:

$Rs=q_v\times[NO_x]/(V_m\times S_{BET}\times m)$

Rs: SCR reaction rates normalized by catalyst surface area, $mol.s^{-1}.m^{-2}$.

q_v: Total gas flow rate, $m^3.s^{-1}$.

$[NO_x]$: Concentration of NO and NO_2 in the inlet streams minus concentration of NO and NO_2 in the outlet streams, ppm.

V_m: The molar volume of reaction gas, $m^3.mol^{-1}$.

S_{BET}: The BET surface areas of the catalysts, $m^2.g^{-1}$.

m: The mass of the catalyst used in activity test, g.

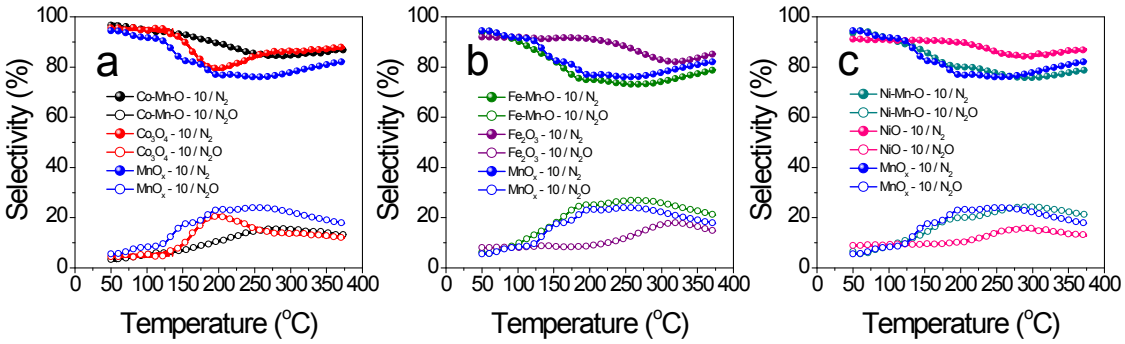

Fig.S13. N_2 and N_2O selectivities as a function of temperature in the NH_3-SCR reaction over (a) Co-Mn-O-10, Co_3O_4-10, MnO_x-10 catalysts, (b) Fe-Mn-O-10, Fe_2O_3-10, MnO_x-10 catalysts and (c) Ni-Mn-O-10, NiO-10, MnO_x-10 catalysts. Reaction conditions: NO = 500 ppm, NH_3 = 500 ppm, O_2 = 2%, GHSV = 30,000 $ml.g^{-1}.h^{-1}$.

The corresponding calculated results are given in Table S4. Among these catalysts, the Mn-based mixed metal oxide catalysts, Co-Mn-O-10, Fe-Mn-O-10 and Ni-Mn-O-10, exhibit large surface areas, which might be beneficial to the NH_3-SCR reaction. Normalized by the BET surface areas, the large NH_3-SCR reaction rates are also obtained over Mn-based mixed metal oxide catalysts at the temperature below 100°C. In contrast, the BET surface areas of Co_3O_4-10, Fe_2O_3-10 and NiO-10 catalysts are small. Simultaneously, their NH_3-SCR reaction rates are also much lower than that of Mn-based mixed metal oxide catalysts. For Co-Mn-O-10 and Fe-Mn-O-10 catalysts, their NH_3-SCR reaction rates are about 7-10 times as much as those of Co_3O_4-10 and Fe_2O_3-10 catalysts, while the NH_3-SCR reaction rate of Ni-Mn-O-10 catalyst is about 20-40 times as much as that of NiO-10 catalyst. It is clear that besides the large surface area, there are plenty of catalytic active species distributed on the surfaces of the Mn-based mixed metal oxide catalysts[8-10]. For the MnO_x-10 catalyst, its BET surface area is quite small, however, the NH_3-SCR reaction rate over MnO_x-10

catalyst is faster than those of Co_3O_4-10, NiO-10 and Fe_2O_3-10 catalysts. This demonstrates that compared with Co_3O_4, NiO and Fe_2O_3, the MnO_x is quite suitable for catalyzing the NH_3-SCR reaction. However, on the other side, the NH_3-SCR reaction rates over Mn-based mixed metal oxide catalysts are higher than that of MnO_x-10 catalyst. This indicates that compared with MnO_x-10 catalyst, Mn-based mixed metal oxide catalysts synthesized via low temperature crystal splitting not only exhibit large surface areas, but also possess abundant catalytic active species on their surfaces.

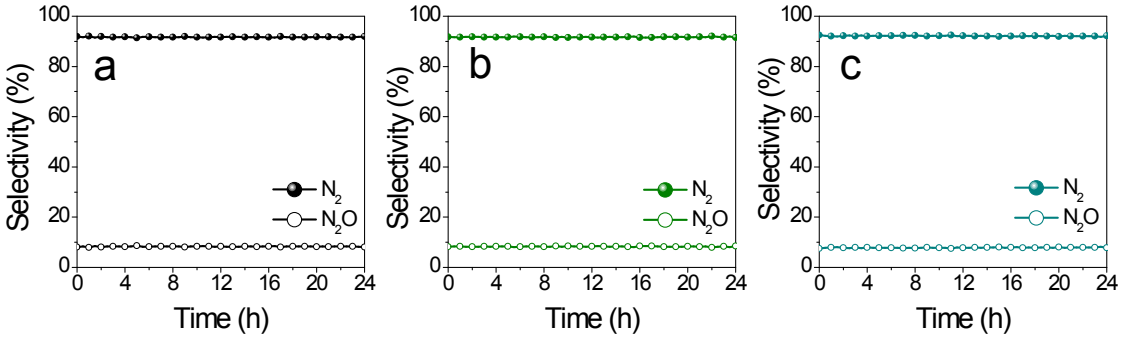

Fig.S14. N_2 and N_2O selectivities as a function of time on stream (temperature: 100 °C) in the NH_3-SCR reaction over (a) Co-Mn-O-10 catalysts, (b) Fe-Mn-O-10 catalysts and (c) Ni-Mn-O-10, catalysts. Reaction conditions: NO = 500 ppm, NH_3 = 500 ppm, O_2 = 2%, GHSV = 30,000 $ml.g^{-1}.h^{-1}$.

The N_2 and N_2O selectivities as a function of temperature and time on stream in the NH_3-SCR reaction over Co-Mn, Fe-Mn, Ni-Mn catalysts have been investigated and the results are shown in Figure S13-S14. Since N_2 and N_2O were the only two N-containing reaction product we have detected during the process of NH_3-SCR reaction, the selectivity of N_2 and N_2O were calculated according to the following equations[11-12]:

$$N_2 \text{ selectivity} = [N_2]_{out}/([N_2]_{out}+[N_2O]_{out}) \times 100\%$$

N_2O selectivity = $[N_2O]_{out}/([N_2]_{out}+[N_2O]_{out}) \times 100\%$

The N_2 and N_2O selectivities as a function of temperature over Co-Mn-O-10, Co_3O_4-10 and MnO_x-10 catalysts has been shown in Figure S13a. For Co-Mn-O-10 catalyst, its N_2 selectivity exceeds 90% when the reaction temperature below 200°C and slowly decreases to 85% in the temperature range from 200°C to 375°C. In contrast, the Co_3O_4-10 catalyst shows its minimum N_2 selectivity 79% at 200°C and the N_2 selectivity of MnO_x-10 catalyst decreases with increasing temperature and maintains its N_2 selectivity at 77% in the temperature range from 200°C to 300°C. It is clear that the N_2 selectivity of Co-Mn-O-10 catalyst is much higher than those of Co_3O_4-10 and MnO_x-10 catalysts over the whole temperature range. Kapteijn et al.[13] have investigated the activity and selectivity of pure manganese oxides for NH_3-SCR reaction and found that the activity and selectivity of N_2 of the manganese oxides were determined by the oxidation state and the degree of crystallinity, the N_2O formation occurs especially on well-ordered manganese oxide crystalline planes due to the presence of high reactive oxygen. Yang et al.[14] and He et al.[15] have claimed the similar conclusion about it. Kröcher et al.[16-17] have found the addition of Nb_2O_5 significantly increased the performance of the MnO_x-CeO_2 catalyst. A clearly superior activity and particularly N_2 selectivity was obtained with the MnNbCe catalyst in comparison to MnO_x-CeO_2. The addition of Nb_2O_5 might decrease the crystallinity of the manganese oxide. In our work, we also found the catalyst Co-Mn-O-10 exhibited much higher catalytic activity and N_2 selectivity than MnO_x-10 catalyst. While in Figure S13b-S13c, the N_2 selectivities of Fe-Mn-O-10 and Ni-Mn-O-10 catalysts are

similar to that of MnO_x-10 catalyst. All their N_2 selectivities reach 95% at 50°C and slowly decrease to 76% in the temperature range from 50°C to 300°C. When temperature exceeds 300°C, their N_2 selectivities have recovered to a certain extent. In contrast, the catalysts Fe_2O_3-10 and NiO-10 exhibit relatively high N_2 selectivities, they maintain at 90% when the temperature below 200°C and gradually decrease to 83-86% in the temperature range from 200°C to 375°C. Obviously, the synergistic effect of cobalt ions and manganese ions enhance the N_2 selectivity of Co-Mn-O-10 catalyst, while iron ions and nickel ions do not have such a synergistic effect with manganese ions.

The N_2 and N_2O selectivities as a function of time on stream (temperature: 100 °C) over Co-Mn-O-10, Fe-Mn-O-10 and Ni-Mn-O-10 catalysts have been shown in Figure S14. In point of catalytic activity, the Co-Mn-O-10 catalyst reaches 100% NO_x conversion at 100°C, meanwhile, Fe-Mn-O-10 catalyst shows 96% NO_x conversion and Ni-Mn-O-10 catalyst exhibits 87% NO_x conversion at this temperature. In Figure S14a-S14c, All these three catalysts show 92% N_2 selectivities and 8% N_2O selectivities during the whole test time (24h). Base on the experimental results of NO_x conversion and N_2 selectivities over Co-Mn-O-10, Fe-Mn-O-10 and Ni-Mn-O-10 catalysts (Figure S13-S14), it seems that they could all exhibit high NO_x conversion and well N_2 selectivities at low reaction temperature (below 100°C).

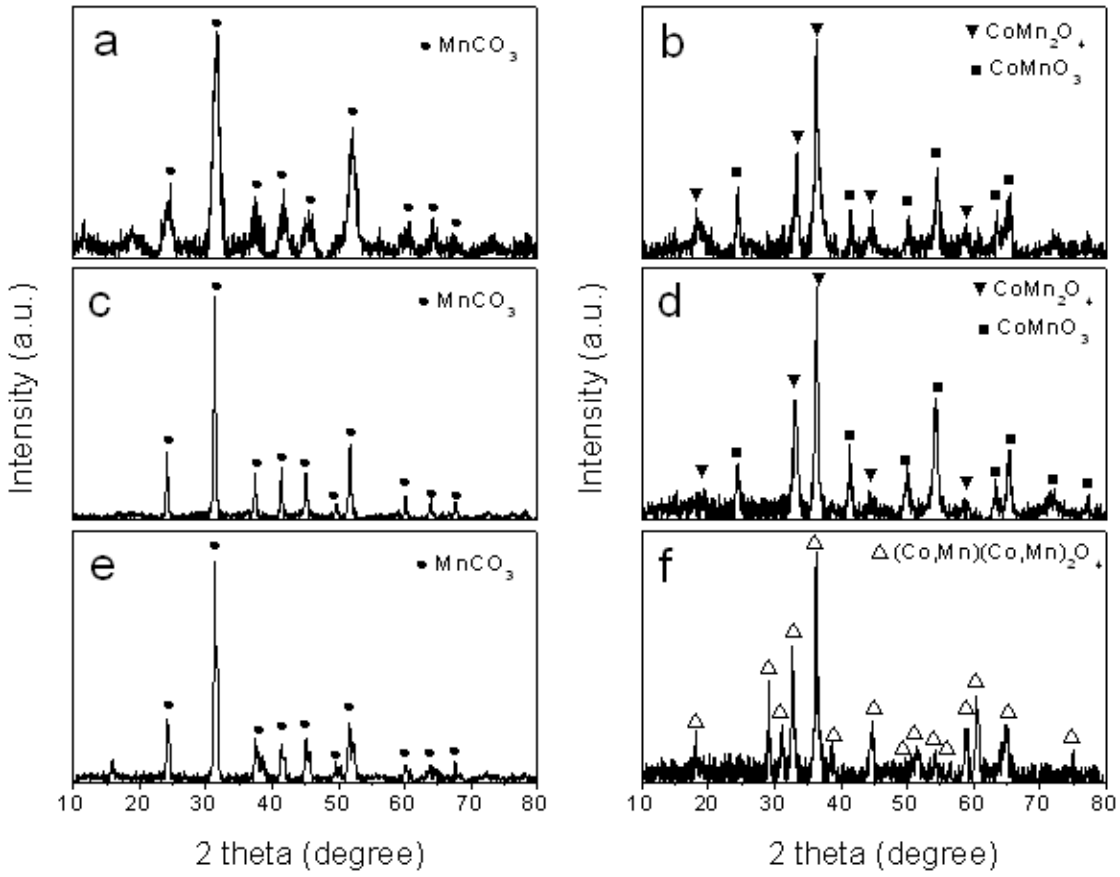

Fig. S15. XRD patterns of cobalt-manganese co-precipitates precipitated at (a) -10°C, (c) 60°C, (e) 160°C (△$MnCO_3$) and the corresponding calcined samples (b) CMO-10, (d) CMO+60, (f) CMO+160.

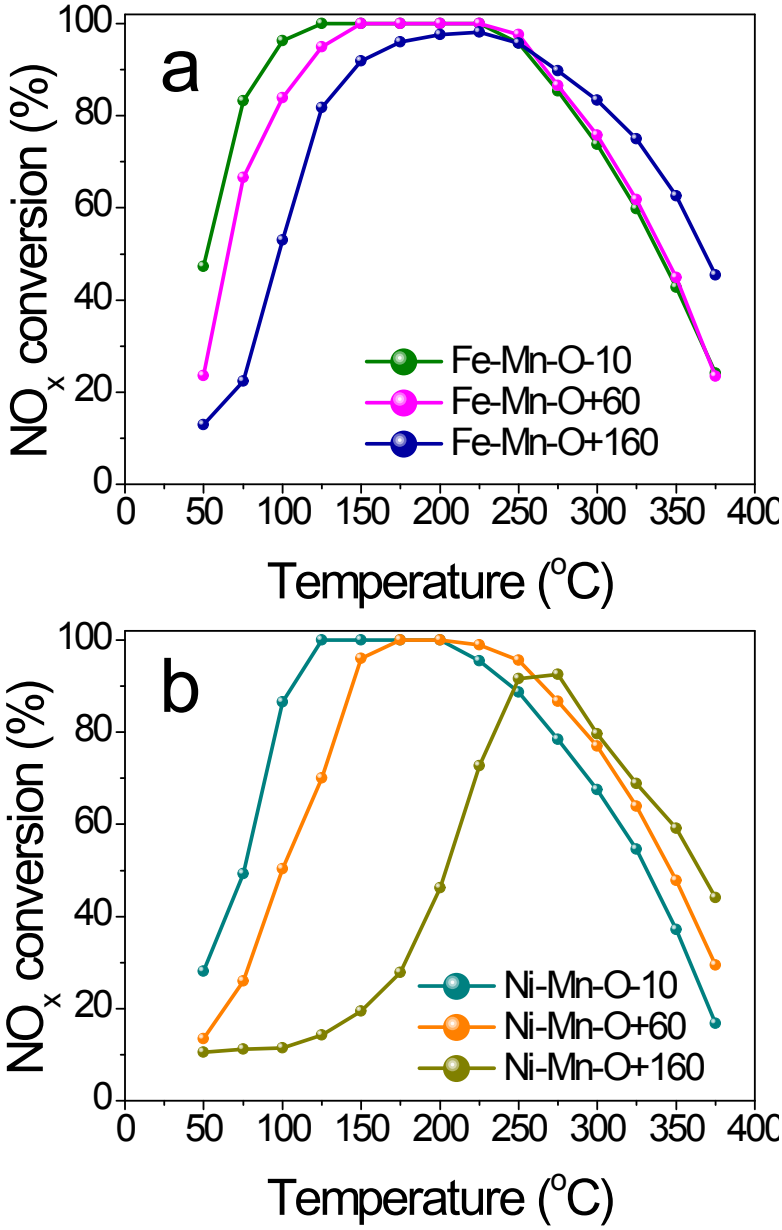

Fig. S16. NO_x conversion as a function of temperature over (a) Fe-Mn-O-10, Fe-Mn-O+60, Fe-Mn-O+160 catalysts and (b) Ni-Mn-O-10, Ni-Mn-O+60, Ni-Mn-O+160 catalysts; Reaction conditions: NO = 400 ppm, NH_3 = 400 ppm, O_2 = 2%,GHSV = 30,000 ml.g^{-1}.h^{-1}.

Fig. S16a depicts the catalytic activities for NH_3-SCR reaction over the Fe-Mn-10, Fe-Mn-O+60, Fe-Mn-O+160 catalysts. In the temperature range of 50-250°C, the catalytic activities of the as-synthesized Fe-Mn-O catalysts decrease with the increase of the co-precipitation temperature. For the Fe-Mn-O+60 catalyst, it shows 24% NO_x conversion at 50°C and 100% NO_x conversion from 150°C to 225°C. As for the Fe-

Mn-O+160 catalyst, it shows 13% NO_x conversion at 50 ^oC and approach maximum NO_x conversion (98%) at 225^oC. Fig.S16b depicts the catalytic activities for NH_3-SCR reaction over the Ni-Mn-10, Ni-Mn-O+60, Ni-Mn-O+160 catalysts. In the temperature range of 50-200^oC, the catalytic activities of the as-synthesized Ni-Mn-O catalysts decrease with the increasing co-precipitation temperature. For Ni-Mn-O+60 catalyst, it shows 13% NO_x conversion at 50^oC and 100% NO_x conversion from 175^oC to 200^oC. While the Ni-Mn-O+160 catalyst shows 11% NO_x conversion at 50^oC and approach maximum NO_x conversion (93%) at 200^oC. By comparing the catalytic activities for NH_3-SCR reaction over the Fe-Mn-O and Ni-Mn-O catalysts prepared at different co-precipitation temperature, the catalytic activities of Fe-Mn-O and Ni-Mn-O catalysts significantly decrease with the increase of the co-precipitation temperature.

REFERENCES

1. M. Kang, E.D. Park, J.M. Kim and J.E. Yie, *Appl. Catal. A:Gen., 2*007, **327**, 261-267.
2. H.T. Zhang and X.H. Chen, *Nanotechnology,* 2006, **17**, 1384-1390.
3. S.C. Petitto, E.M. Marsh, G.A. Carson and M.A. Langell, *J. Mol. Catal. A-Chem.*, 2008, **281**, 49-58.
4. S.C. Petitto and M.A. Langell, *J. Vac. Sci. Technol. A*, 2004, **22**, 1690-1696.
5. J.L. Gautier, E. Rios, M. Gracia, J.F. Marco and J.R. Gancedo, *Thin Solid Films*, 1997, **311**, 51-57.
6. L. Zhou, D.Y. Zhao and X.W. Lou, *Adv. Mater.,* 2012, **24**, 745-748.
7. F. Liu, H. He, C. Zhang, Z. Feng, L. Zheng, Y. Xie and T. Hu, *Appl. Catal. B: Environ.*, 2010, **96**, 408.
8. Q. Lin, J. Li, L. Ma and J. Hao, *Catal. Today,* 2010**, 151**, 251.
9. B. Thirupathi and P. G. Smirniotis, *Appl. Catal. B: Environ.*, 2011, **110**, 195.
10. B. Thirupathi and P. G. Smirniotis, *J. Catal.*, 2012, **288**, 74.
11. Z. Chen, Q. Yang, H. Li, X. Li, L. Wang and S. C. Tsang, *J. Catal*., 2010, **276**, 56.
12. X.L. Mou, B.S. Zhang, Y. Li, L.D. Yao, X.J. Wei, D.S. Su and W.J. Shen, *Angew. Chem. Int. Ed.*, 2012, **51**, 2989.
13. F. Kapteijn, L. Singoredjo and A. Andreini, *Appl. Catal. B: Environ.*, 1994, **3**, 173.

14. G. Qi, R. T. Yang and R. Chang, *Appl. Catal. B: Environ*., 2004, **51**, 93.
15. Z. Lian, F. Liu, H. He, X. Shi, J. Mo and Z. Wu, *Chem. Eng. J.*, 2014, **250**, 390.
16. M. Casapu, O. Kröcher and M. Elsener, *Appl. Catal. B: Environ.*, 2009, **88**, 413.
17. M. Casapu, O. Kröcher, M. Mehring, M. Nachtegaal, C. Borca, M. Harfouche and D. Grolimund, *J. Phys. Chem. C.*, 2010, **114**, 9791.